Original Article

JCBFM

Journal of Cerebral Blood Flow & Metabolism
2018, Vol. 38(5) 904–918
© Author(s) 2017
Reprints and permissions:
sagepub.co.uk/journalsPermissions.nav
DOI: 10.1177/0271678X17709709
journals.sagepub.com/home/jcbfm
SAGE

Insulin differentially affects the distribution kinetics of amyloid beta 40 and 42 in plasma and brain

Suresh Kumar Swaminathan[1,2], Kristen M Ahlschwede[1,3], Vidur Sarma[1,2], Geoffry L Curran[2,3], Rajesh S Omtri[1], Teresa Decklever[2], Val J Lowe[2], Joseph F Poduslo[3] and Karunya K Kandimalla[1,3]

Abstract

Impaired brain clearance of amyloid-beta peptides (Aβ) 40 and 42 across the blood–brain barrier (BBB) is believed to be one of the pathways responsible for Alzheimer's disease (AD) pathogenesis. Hyperinsulinemia prevalent in type II diabetes was shown to damage cerebral vasculature and increase Aβ accumulation in AD brain. However, there is no clarity on how aberrations in peripheral insulin levels affect Aβ accumulation in the brain. This study describes, for the first time, an intricate relation between plasma insulin and Aβ transport at the BBB. Upon peripheral insulin administration in wild-type mice: the plasma clearance of Aβ40 increased, but Aβ42 clearance reduced; the plasma-to-brain influx of Aβ40 increased, and that of Aβ42 reduced; and the clearance of intracerebrally injected Aβ40 decreased, whereas Aβ42 clearance increased. In hCMEC/D3 monolayers (in vitro BBB model) exposed to insulin, the luminal uptake and luminal-to-abluminal permeability of Aβ40 increased and that of Aβ42 reduced; the abluminal-to-luminal permeability of Aβ40 decreased, whereas Aβ42 permeability increased. Moreover, Aβ cellular trafficking machinery was altered. In summary, Aβ40 and Aβ42 demonstrated distinct distribution kinetics in plasma and brain compartments, and insulin differentially modulated their distribution. Cerebrovascular disease and metabolic disorders may disrupt this intricate homeostasis and aggravate AD pathology.

Keywords

Alzheimer's disease, blood–brain barrier, SPECT, pharmacokinetics, endothelium, cerebrovascular disease, insulin, diabetes

Received 22 July 2016; Revised 18 March 2017; Accepted 24 March 2017

Introduction

Alzheimer's disease (AD) is characterized by amyloid beta (Aβ) deposits in the brain parenchyma; intraneuronal tangles of hyperphosphorylated tau protein; neurodegeneration in the cortex and hippocampus; and impaired glucose metabolism in the brain.[1] Investigators have been targeting these hallmarks of AD pathology with an expectation to uncover novel therapeutic strategies to halt or even reverse AD progression. Among these, the reduction of brain Aβ burden is widely considered to be a viable therapeutic strategy, and developing methods to promote brain Aβ clearance have been at the forefront of AD research. The two-hit vascular hypothesis of AD, proposed by Zlokovic, posits that Aβ accumulation in the brain is secondary and subsequent to the primary insult sustained by the cerebral vasculature.[2] There is substantial speculation on the pathological changes that are

[1]Department of Pharmaceutics and Brain Barriers Research Center, College of Pharmacy, University of Minnesota, Minneapolis, MN, USA
[2]Department of Radiology, Mayo Clinic College of Medicine, Rochester, MN, USA
[3]Department of Neurology, Mayo Clinic College of Medicine, Rochester, MN, USA

Corresponding author:
Karunya K Kandimalla, Department of Pharmaceutics and Brain Barriers Research Center, University of Minnesota, Minneapolis, MN 55455, USA.
Email: kkandima@umn.edu

capable of delivering the first hit to the cerebral vasculature, and some of the likely suspects include hyperinsulinemia and peripheral insulin resistance, that are prevalent in type II diabetes.[3]

Hyperinsulinemia is believed to engender cerebrovascular dysfunction and dampen cerebrovascular reactivity, which is critical for sustaining neuronal activity.[4] Clinically, cerebrovascular dysfunction is measured as changes in the cerebral blood flow and alterations in the permeability of the cerebrovascular endothelium, classically referred to as the blood–brain barrier (BBB). The cerebrovascular reactivity is primarily facilitated by the BBB and vascular smooth muscle in the larger vessels. But in the smaller vessels, such as capillaries that are devoid of smooth muscle cells, contractile pericytes take their place.[5] Moreover, pericytes are believed to restrict vascular permeability and maintain the BBB integrity.[6,7] Hyperinsulinemia could lead to the degeneration of these vascular cells, cause disruptions in cerebrovascular structure and function, and lead to BBB dysfunction.[8]

The BBB endothelium is a quintessential trafficking portal that delivers critical cargo, including glucose and growth factors, from plasma to brain, and clear metabolic byproducts, such as Aβ peptides, from the brain. Previous studies have shown that insulin impacts plasma pharmacokinetics of Aβ peptides and modulates the dynamics Aβ trafficking at the BBB.[9–11] Elucidating the cellular and molecular mechanisms harnessed by insulin in order to influence Aβ trafficking at the BBB in healthy animals is critical to fully realize the consequences of BBB dysfunction triggered by insulin resistance and hyperinsulinemia. Hence, the purpose of this study is to investigate the effect of insulin on the distribution kinetics of two main Aβ isoforms, Aβ40 and Aβ42, in plasma and brain compartments, with an emphasis on the impact of insulin exposure on the Aβ trafficking across the BBB endothelium.

Materials and methods

Reagents and lab supplies

Aβ40 and Aβ42 peptides were synthesized in the Mayo Clinic Proteomics Core (Rochester, MN) or procured from AAPPtec, LLC (Louisville, KY). The ^{125}I was obtained from Perkin Elmer Life and Analytical Sciences (Boston, MA). Insulin (Novolin® R or Humulin® R) was purchased from Eli Lilly (Indianapolis, IN). Plastic wares were obtained from Corning life sciences (Tewksbury, MA), USA Scientific (Ocala, FL) or Denville Scientific Inc., (South Plainfield, NJ). Plasmids were obtained from Addgene (Cambridge, MA). All other reagents were purchased from Sigma-Aldrich (St. Louis, MO) unless stated otherwise.

Animals

Wild-type (WT) mice (B6SJLF1) were purchased from Jackson Laboratory, Bar Harbor, ME. They were housed in Mayo Clinic animal care facility under standard conditions and provided access to food and water ad libitum. Male and female mice between ages five and eight months were used. The male and female mice were randomly distributed to various groups. The animal studies were done in a single-blinded fashion. The animal experimenters were provided with minimal details required for the experiment to be performed. In addition, they were blinded from details of the final data analysis and the study conclusions until all animal experiments were completed. All studies were conducted in accordance with the National Institutes of Health guidelines for the care and use of laboratory animals, and protocols approved by the Mayo Clinic Institutional Animal Care and Use Committee. Data in this manuscript are reported according to the ARRIVE guidelines.

Radioiodination of Aβ peptides

As described in our previous publications,[12,13] the Aβ peptides were labeled with ^{125}I using the chloramine-T reaction, and the product was dialyzed to remove unconjugated ^{125}I. The purity of the ^{125}I-labeled protein was determined by trichloroacetic acid (TCA) assay.

Biodistribution of ^{125}I-Aβ

B6SJLF1 mouse was anesthetized (1.5% isoflurane with 4 L/min O_2) and its femoral vein/artery and the internal carotid artery were catheterized. Saline (100 μL, control) or insulin (nominal dose of 1 IU, treatment) was administered via internal carotid artery over the course of 5 min. Fifteen minutes following the insulin infusion, 100 μCi of ^{125}I-Aβ40 or ^{125}I-Aβ42 was administered to each mouse via the femoral vein (note ^{125}I-Aβ42: saline (n = 6) and insulin (n = 7); ^{125}I-Aβ40 saline (n = 3) and insulin (n = 3)). A 20-μL blood sample was collected from the femoral artery at pre-determined time points (0.25, 1, 3, 5, 7, 10, and 15 min post administration of ^{125}I-Aβ); the plasma was separated; TCA precipitated; and the radioactivity of the intact protein was measured in the pellet by a two-channel gamma counter (Cobra II; Amersham Biosciences Inc., Piscataway, NJ). Finally, the mouse was transcardially perfused with excess phosphate-buffered saline (PBS) to flush radioactivity in the blood, and the brain radioactivity was assayed.

The plasma data at each time point were analyzed by Grubb's test to remove potential statistical outliers. The average plasma data was then computed and then fitted to the following biexponential equation

using WinNonlin® (Pharsight, Mountain View, CA)

$$Cp = Ae^{-\alpha t} + Be^{-\beta t} \quad (1)$$

and the primary parameters – A and B intercepts, as well as the α and β rate constants were estimated. The secondary parameters such as the C_{max} (maximum plasma concentration), plasma clearance (CL), and area under the plasma concentration curve (AUC) were calculated also using WinNonlin.

The influx of ^{125}I-Aβ proteins into the brain was determined as described below:

$$\text{Brain influx} = \frac{Brain\ radioactivity\ (\mu Ci)}{Plasma\ AUC\ \left(\frac{\mu Ci}{mL}\right) * min} \quad (2)$$

To resolve insulin's impact on the ^{125}I-Aβ influx in various brain regions of the left and right brain hemispheres, the experiment was conducted by infusing a higher dose of insulin (4.2 IU) over 15 min via the left internal carotid artery. Then, 100 μCi of ^{125}I-Aβ40 or ^{125}I-Aβ42 was administered to each mouse via the femoral vein (^{125}I-Aβ42: saline (n = 6) and insulin (n = 5); ^{125}I-Aβ40 saline (n = 5, one outlier was excluded) and insulin (n = 6, one outlier was excluded)), and the plasma was sampled from the femoral artery for the following 15 min. At the end of the experiment, each hemisphere was dissected into the cortex, hippocampus, caudate putamen, thalamus, brain stem, and cerebellum, and the radioactivity was assayed in the gamma counter.

Dynamic SPECT/CT studies to assess ^{125}I-Aβ distribution in plasma and brain compartments

For assessing plasma-to-brain influx, the WT mice (n = 3) were infused with saline or insulin (4.2 IU) for 15 min via the internal carotid artery and then administered with 100 μCi of ^{125}I-Aβ40 or ^{125}I-Aβ42 through the femoral vein. The animals were immediately imaged for the following 40 min by dynamic SPECT/CT (Gamma Medica, Northridge, CA) as described previously.[13] The plasma-to-brain influx of ^{125}I-Aβ was predicted by Gjedde–Patlak plot,[14–16] which was constructed by plotting

$$\frac{Amount_{brain}\ (t)}{C_p\ (t)} \quad Vs. \quad \frac{\int_0^t C_p(\tau)\mathrm{d}\tau}{C_p\ (t)} \quad (3)$$

The $Amount_{brain}$ denotes the brain radioactivity at time t; the $\int_0^t C_p(\tau)\mathrm{d}\tau$ is plasma AUC from the time of injection; and $C_p\ (t)$ is instantaneous plasma activity at time = t. Plasma concentrations were simulated using equation (1), and predicted primary plasma PK parameters. The $\frac{\int_0^t C_p(\tau)\mathrm{d}\tau}{C_p\ (t)}$ is also referred to as exposure time. Slope of the linear portion of the Gjedde–Patlak plot is referred to as the brain transfer rate constant (K_i).

To assess brain-to-plasma clearance, mice were administered with saline or a nominal dose of 4.2 IU insulin (four animals per group) via the internal carotid artery over 15 ± 1 min. At the end of infusion, they were injected with 1 μL of either ^{125}I-Aβ40 or ^{125}I-Aβ42 (about 3–4 μCi /per animal) into the right hippocampus. The animals were imaged for the following 100 min by dynamic SPECT/CT. The obtained radioactivity counts were normalized to the body weight and the administered radioactivity. Changes in the brain radioactivity (as a percent of initial levels) were plotted on the natural log scale against time and then fitted to a one-phase decay model using Prism version 5 (Graph pad software, La Jolla, CA).

Cell culture

The immortalized human cerebral microvascular endothelial cell line (hCMEC/D3) was a kind gift from P-O Couraud, Institut Cochin, France. These cells were cultured as previously described.[17]

Determination of ^{125}I-Aβ flux in hCMEC/D3 monolayers

Cells were cultured on Transwell® inserts (Corning, Tewksbury, MA) for seven to nine days to form a polarized monolayer. The monolayer integrity was verified by monitoring the transendothelial electric resistance (TEER). The ^{125}I-Aβ transport studies were conducted when TEER values ranged between 80 and 120 Ω/cm^2.

Cell monolayers were serum-starved overnight using growth media containing low serum (1% v/v fetal bovine serum) before pre-treatment with 100 mIU/mL insulin on the luminal side for 20 min at 37°C. Then ^{125}I-Aβ40 or ^{125}I-Aβ42 (20 μCi/mL) was pre-mixed with 12.8 μg/mL of activated alpha-2 M for 30 min, and 500 μL of the mixture was added to the luminal compartment at the start of the experiment (t = 0 min). A 20-μL aliquot of the medium was sampled from the abluminal compartment at t = 10, 20, 30, 45, 60 and 90 min and assayed for radioactivity. The cumulative amount of radioactivity reaching the abluminal compartment was plotted against time. The slope of the regression line indicates luminal-abluminal flux of ^{125}I-Aβ tracer. The apparent permeability of ^{125}I-Aβ was obtained by normalizing the flux with initial donor concentration.

To assess abluminal-to-luminal permeability (A-L), insulin (100 mIU/mL) and ^{125}I-Aβ (20 μCi/mL) were added to the abluminal compartment and 20-μL samples were collected from the luminal compartment at various time intervals. A-L permeability was then calculated as described above.

DNA transfections

Cells, cultured on 6-well plates or 35-mm glass bottom culture dishes (MatTek Corp, Ashland, MA), were transfected with 1.5–2 μg of human insulin receptor plasmid (IR, Addgene plasmid #24049, 0.67 or 1.1 μg/μL in 1X Tris-EDTA buffer) using Lipofectamine LTX reagent kit (Invitrogen, Grand Island, NY). The DNA was diluted with 145 μL Opti-MEM™ (Invitrogen) and 2.5 μL of Plus reagent was added. The contents were mixed by pipetting and then transferred to another tube containing 6 μL of Lipofectamine® pre-diluted with 144 μL of Opti-MEM™. The mixture was added to the cells and replaced with fresh growth media after 12 h. Then, cells were allowed to recover for 36 h before the experiment.

Impact of insulin on FITC-transferrin uptake by flow cytometry

The IR transfected cells were exposed to insulin (100 mIU/mL, 20 min) and then treated with 40 μg/mL fluorescein isothiocyanate-conjugated transferrin (FITC-transferrin) for 30 min at 37°C. The cells were harvested, fixed with 2% v/v para-formaldehyde for 15 min, and the intracellular fluorescence was measured using Accuri™ C6 flow cytometer (BD Biosciences, San Jose, CA).

Impact of insulin on Alexa Fluor® 647-conjugated cholera toxin and Alexa Fluor® 633-conjugated transferrin by confocal microscopy

The IR transfected cells were treated with insulin (100 mIU/mL, 20 min) and then treated with Alexa Fluor® 647-conjugated cholera toxin (AF647-CT) (15 μg/mL) or Alexa Fluor® 633-conjugated Transferrin (AF633-Trf) (10 μg/mL) for 30 min. The treatments were removed and then the cells were washed twice with cold Hanks Balanced Salt Solution (HBSS). Subsequently, the cells were treated with an ice cold solution of 0.2 M acetic acid and 0.5 M sodium chloride (pH 2.5) for 5 min (two exchanges, each for 2 min and one exchange for 1 min) to strip the cell membrane-bound fluorescent probes. The cells were then neutralized with ice-cold HBSS, fixed with 4% v/v para-formaldehyde in PBS for 30 min at room temperature and then extensively washed with PBS. The cells were then washed thoroughly with PBS, incubated with 0.2 μg/mL Hoechst 33342 (Life technologies, Grand Island, NY) for 5 min and washed again with PBS. The dishes were air-dried, mounted with ProLong® gold antifade reagent (Life technologies, Grand Island, NY) and then imaged by confocal microscopy (Zeiss LSM 780 laser confocal microscope equipped with C-Apochromat 40X/1.2 W objective).

Impact of insulin on ^{125}I-Aβ exocytosis

Polarized hCMEC/D3 monolayers were cultured on 24-mm Transwell® inserts and exposed to 100 mIU/mL insulin for 20 min. Then, both luminal and abluminal chambers were spiked with ^{125}I-Aβ40 or ^{125}I-Aβ42 (10 μCi) and incubated for 1 h at 37°C. The media was removed, filter surface was washed twice with HBSS to remove non-specifically bound radioactive peptides, and then the cells were fed with growth media containing 1% FBS (control) or 100 mIU/mL insulin (treatment). Then, 50-μL sample aliquots were obtained from the luminal and abluminal chambers at 10, 20, 30, 45, 60 and 90 min, and assayed for radioactivity.

Whole cell lysis, plasma membrane fractionation, and Western blotting

Whole cell lysis: Control or insulin (100 mIU/mL, 20 min)-treated cells were washed with ice-cold Dulbecco's PBS, dislodged from tissue culture dishes using a cell scrapper, pelleted and then dispersed in radioimmunoprecipitation assay buffer (RIPA, Thermo Scientific, Waltham, MA) containing EDTA-free protease inhibitor cocktail (Roche, Branford, CT). Protein lysates were obtained by a high-speed centrifugation at 9600 *g*, 5 min, 4°C.

Plasma membrane fractionation, western blotting, and immunocytochemistry: Methods have been detailed in the Supplementary Section.

Statistical analyses

Statistical significance ($*p < 0.05$, $**p < 0.01$, $***p < 0.001$) of the differences between the mean responses with and without insulin exposure, both in vivo as well as in vitro, was ascertained by Student's *t*-test using Prism version 5 (Graph pad software, La Jolla, CA). Significance ($*p < 0.05$, $**p < 0.01$, $***p < 0.001$) of insulin impact on the influx of ^{125}I-Aβ in various brain regions was evaluated by two-way ANOVA followed by Bonferroni's multiple comparison tests. In dynamic SPECT studies, F-tests were done to compare the statistical significance of the curves obtained with and without insulin exposure.

Results

Effect of insulin on the plasma pharmacokinetics of Aβ peptides in mice

Both ^{125}I-Aβ40 (Figure 1(a)) and ^{125}I-Aβ42 (Figure 1(b)) displayed biexponential plasma disposition in mice treated with insulin or saline. Maximal plasma concentration (C_{max}) and area under the curve (AUC)

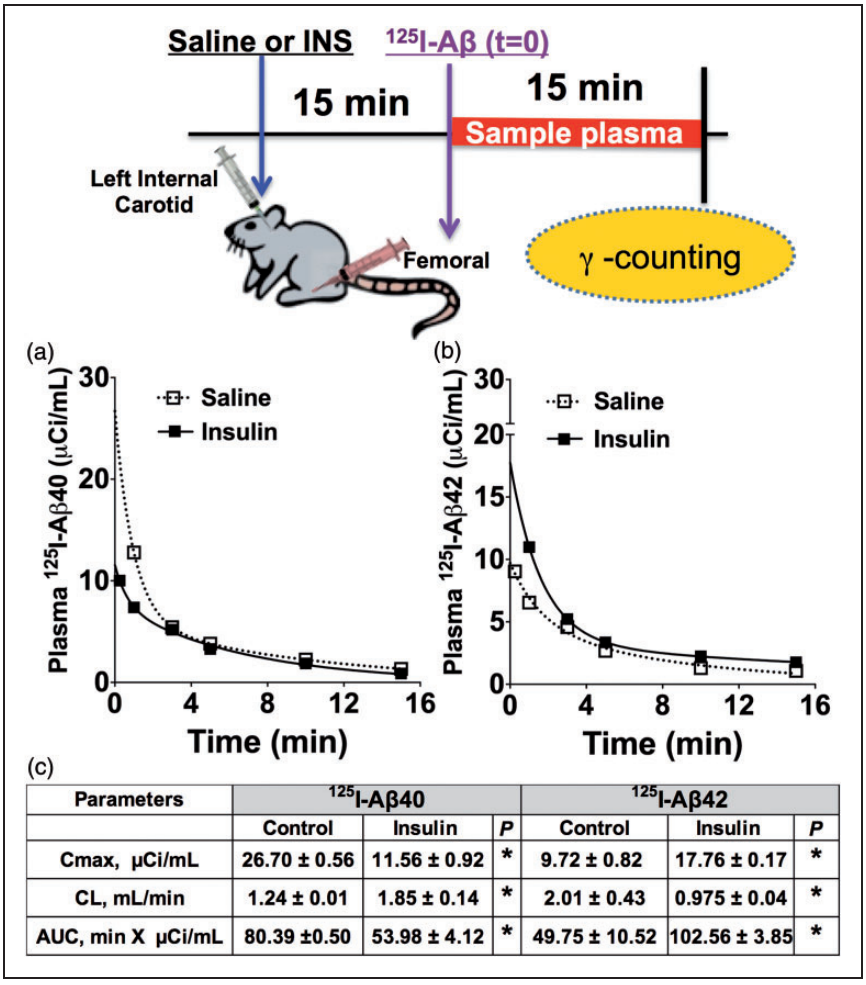

(c)

Parameters	^{125}I-Aβ40			^{125}I-Aβ42		
	Control	Insulin	P	Control	Insulin	P
Cmax, μCi/mL	26.70 ± 0.56	11.56 ± 0.92	*	9.72 ± 0.82	17.76 ± 0.17	*
CL, mL/min	1.24 ± 0.01	1.85 ± 0.14	*	2.01 ± 0.43	0.975 ± 0.04	*
AUC, min X μCi/mL	80.39 ±0.50	53.98 ± 4.12	*	49.75 ± 10.52	102.56 ± 3.85	*

Figure 1. Plasma clearance of (a) ^{125}I-Aβ40 increased and (b) ^{125}I-Aβ42 clearance decreased in insulin pre-administered B6SJLF1 mice. Graphs depict the plasma pharmacokinetics of ^{125}I-Aβ fitted to a two-compartment model. (c) Predicted plasma pharmacokinetic parameters are presented in the table as mean ± S.E. (Aβ40: saline (n = 3), insulin (n = 3); Aβ42: saline (n = 6), insulin (n = 7)). *$p < 0.05$: Student's *t*-test.
AUC: area under the curve; Cmax: maximum plasma concentration; CL: plasma clearance.

of ^{125}I-Aβ40 were found to be significantly lower in insulin pre-injected animals than in control animals (Figure 1(c)). However, the C_{max} and AUC of ^{125}I-Aβ42 significantly increased in insulin-treated mice compared to the control mice (Figure 1(c)). Similarly, ^{125}I-Aβ40 clearance increased, but ^{125}I-Aβ42 clearance decreased in insulin-treated animals compared to controls (Figure 1(c)).

Insulin modulates the plasma-to-brain distribution of ^{125}I-Aβ40 and ^{125}I-Aβ42

The parameter obtained by normalizing the brain uptake of intravenously administered ^{125}I-Aβ with its plasma AUC indicates the plasma-to-brain influx. A 15-min infusion of 1 IU insulin via the left internal carotid artery was shown to increase the influx of ^{125}I-Aβ40 but reduced the influx of ^{125}I-Aβ42 as compared to saline-treated controls (Figure 2(a)). At higher doses (4.2 IU), the effect of insulin was significant in various brain regions of the left and right brain hemispheres (Figure 2(b)). The ^{125}I-Aβ40 influx into various brain regions (cortex, hippocampus, thalamus and caudate putamen) of the left hemisphere, which received higher insulin exposure (Supplementary Figure 1), was statistically significant compared to the control mice (Figure 2(b)). In contrast, the influx of ^{125}I-Aβ42 significantly decreased in the left hemisphere of insulin pre-injected mice compared to the control mice. Although similar trends were apparent in the right hemisphere, they are not statistically significant (Figure 2(b)).

These intriguing results were further verified using dynamic SPECT imaging. The plasma-to-brain transfer rate constant (K_i) of ^{125}I-Aβ40 was found to be higher (Figure 3(a)), but the K_i of ^{125}I-Aβ42 was lower

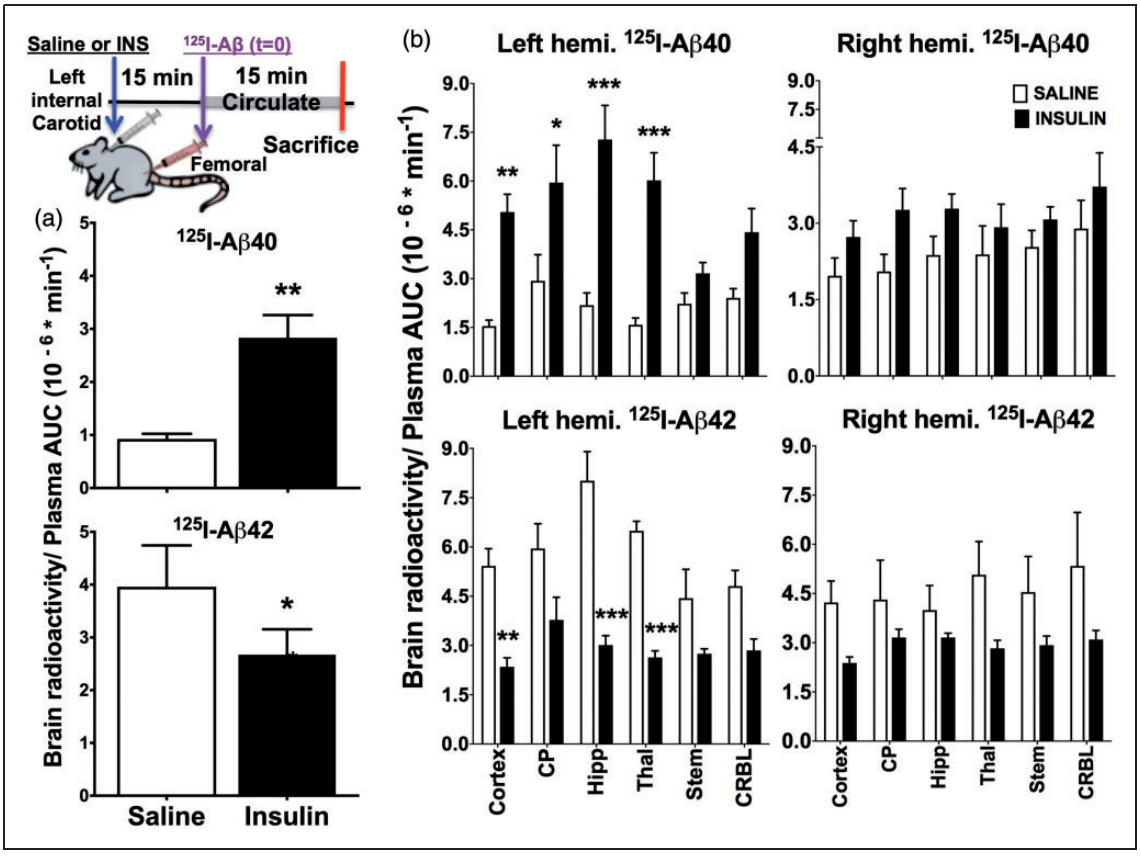

Figure 2. Brain influx of ^{125}I-Aβ40 increased and ^{125}I-Aβ42 decreased in insulin-treated B6SJLF1 mice. Normal saline or insulin (INS) was infused into the left internal carotid artery such that the left brain hemisphere received approximately two-fold greater insulin exposure than the right hemisphere. Then ^{125}I-Aβ was administered via femoral vein, which is equally distributed to both left and right brain hemispheres. This experimental modality allows us to relate the extent of insulin exposure to changes in the influx of ^{125}I-Aβ. (a) The brain influx values of ^{125}I-Aβ in mice infused with 1 IU of insulin over 15 min. Data are presented as mean ± S.D. (n = 3); *$p < 0.05$, Student's *t*-test. (b) The brain influx of ^{125}I-Aβ into various brain regions of mice infused with 4.2 IU of insulin over 15 min. Data are presented as mean ± S.D. (Aβ40: saline (n = 5), insulin (n = 6); Aβ42: saline (n = 6), insulin (n = 5)). Two-way ANOVA followed by Bonferroni's multiple comparison test was conducted to evaluate if the differences between saline and insulin-treated mice are significant in various brain regions. *$p < 0.05$, **$p < 0.01$, and ***$p < 0.001$.

(Figure 3(b)) in the insulin-infused mice compared to saline-infused mice. The K_i of ^{125}I-Aβ40 was 4.85 ± 0.24 mL * min^{-1} * 10^{-3} in control mice and it increased to 5.95 ± 0.15 mL * min^{-1} * 10^{-3} in insulin-treated animals. The K_i of ^{125}I-Aβ42 was 9.97 ± 0.22 mL * min^{-1} * 10^{-3} in control mice and it decreased to 7.92 ± 0.18 * mL * min^{-1} * 10^{-3} in insulin-treated animals.

Insulin modulates the brain-to-plasma clearance of ^{125}I-Aβ40 and ^{125}I-Aβ42 in mice

Saline or insulin was infused via the internal carotid artery and then ^{125}I-Aβ40 or ^{125}I-Aβ42 was injected into the right hippocampus. Change in the injected radioactivity with time was monitored by SPECT/CT imaging (Figure 4(a)). The brain elimination rate constant of ^{125}I-Aβ40 was 0.009 ± 0.001 min^{-1} in control mice but decreased to 0.003 ± 0.001 min^{-1} in insulin-treated mice (Figure 4(a), panel-i). In contrast, the brain elimination of ^{125}I-Aβ42 in the control mice was 0.006 ± 0.001 min^{-1} but increased to 0.011 ± 0.002 min^{-1} in mice pre-administered with insulin (Figure 4(a), panel-ii). Representative SPECT/CT images are presented in Figure 4(b).

Insulin alters the transcytosis and exocytosis of ^{125}I-Aβ40 and ^{125}I-Aβ42 in vitro

Insulin pre-treatment on the luminal side increased the L-A permeability of ^{125}I-Aβ40 from 14.4 ± 2.7 cm * min^{-1} *10^{-5} measured in untreated hCMEC/D3 monolayers to 20.9 ± 6.2 cm*min^{-1} *10^{-5} (Figure 5(a), panel-i). But the permeability of ^{125}I-Aβ42 decreased from 3.39 ± 0.57 cm * min^{-1} *10^{-5} in the control monolayers to 2.32 ± 0.38 cm * min^{-1} *10^{-5} in the

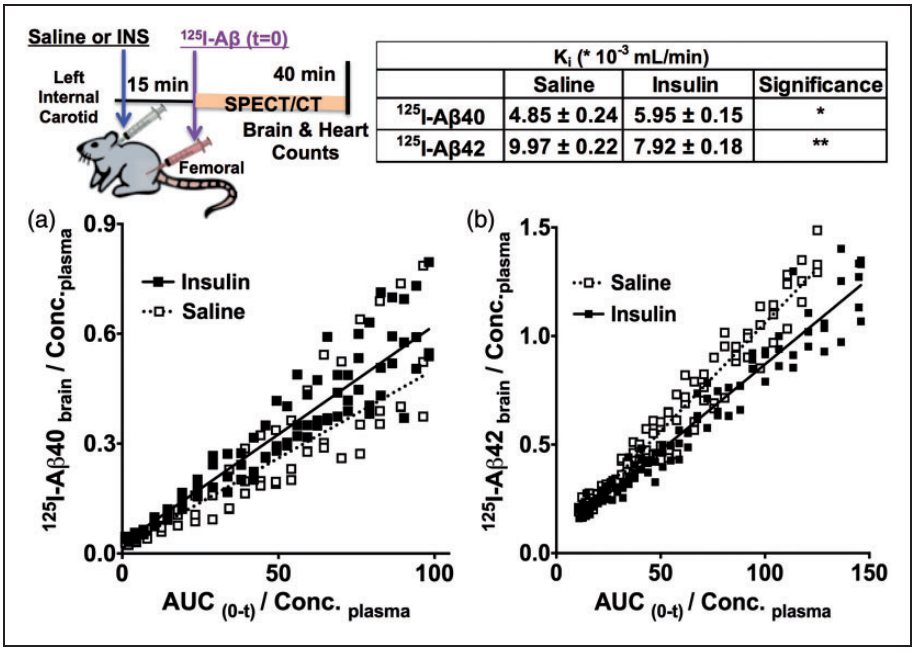

Figure 3. Determination of plasma-to-brain influx of ^{125}I-Aβ proteins by SPECT imaging. Saline or insulin (INS) was infused into the left internal carotid artery, followed by IV bolus administration of ^{125}I-Aβ via femoral vein. Dynamic SPECT/CT imaging of mice was pursued immediately after ^{125}I-Aβ administration. The brain transfer rate constants (K_i) of (a) ^{125}I-Aβ40 and (b) ^{125}I-Aβ42 were obtained from the slopes of Gjedde–Patlak plots. The data are presented as mean ± S.D. (n = 3). Significance of the differences between the brain influx (slope) of ^{125}I-Aβ in saline and insulin infused mice was evaluated by F-test. ^{125}I-Aβ40: $F(2,140) = 12.56$, $p < 0.0001$ and ^{125}I-Aβ42: $F(2,190) = 70.02$, $p < 0.0001$.

insulin-treated monolayers (Figure 5(a), panel-ii). Similarly, insulin treatment on the abluminal side decreased the A-L permeability of ^{125}I-Aβ40 from 17.86 ± 1.67 cm*min^{-1} *10^{-5} to 14.46 ± 0.43 cm * min^{-1} *10^{-5} (Figure 5(a), panel-iii). But the A-L permeability of ^{125}I-Aβ42 increased in the insulin-treated monolayers, from 2.97 ± 0.50 cm * min^{-1} *10^{-5} to 3.51 ± 0.25 cm * min^{-1} *10^{-5} (Figure 5(b), panel-iv). These in vitro observations were in agreement with the results obtained in vivo.

Subsequently, we investigated if the internalized ^{125}I-Aβ isoforms are exocytosed differently from the hCMEC/D3 monolayers. ^{125}I-Aβ40 was exocytosed to both luminal and abluminal chambers. However, the rate of exocytosis into the abluminal chamber (263.88 ± 54.81 μCi * min^{-1}) was significantly greater than that into the luminal chamber (84.41 ± 7.2 μCi * min^{-1}) (Figure 5(b), control treatments in panels-i and iii; note: Y-axis scales are different in these plots). Upon insulin treatment, the luminal exocytosis rate of ^{125}I-Aβ40 decreased to 56.52 ± 12.20 μCi * min^{-1} (Figure 5(b), panel-i) and the abluminal exocytosis rate increased to 526.70 ± 183.52 μCi * min^{-1} (Figure 5(b), panel-iii). Although no significant differences were noted between the luminal (79.51 ± 10.71 μCi * min^{-1}) and abluminal (79.07 ± 52.37 μCi * min^{-1}) exocytosis rates of ^{125}I-Aβ42 (Figure 5(b), control treatments in panels-ii and iv), with insulin treatment, only the exocytosis of ^{125}I-Aβ42 to the luminal side significantly increased to 129.11 ± 48.85 μCi * min^{-1} (Figure 5(b), panel-ii).

Insulin exposure triggers Aβ receptor/transporter relocation in hCMEC/D3 monolayers

The fate of putative amyloid receptors/transporters, such as LRP-1, RAGE, SRB-1 and P-gp,[18–20] upon insulin exposure, was investigated in hCMEC/D3 cells. The levels of LRP-1, RAGE and P-gp increased in the plasma membrane fraction of insulin-treated cells compared to that of the control cells, but SRB-1 levels were not affected by the insulin exposure (Figure 6(a), panel-i). However, insulin pre-treatment did not change the whole cell expression levels of these receptors (Figure 6(a), panel-ii).

Subsequently, the effect of insulin on the re-distribution of Aβ receptors LRP-1 and RAGE, as well P-gp efflux transporter within hCMEC/D3 monolayers was imaged by confocal microscopy (Figure 6(b), panels i to iii). With insulin pre-treatment, LRP-1 accumulation in the plasma membrane increased and reached the highest levels upon 20 min of insulin exposure. However, the LRP-1 immunofluorescence decreased upon further exposure to insulin for 60 min (Figure 6(b), panel-i).

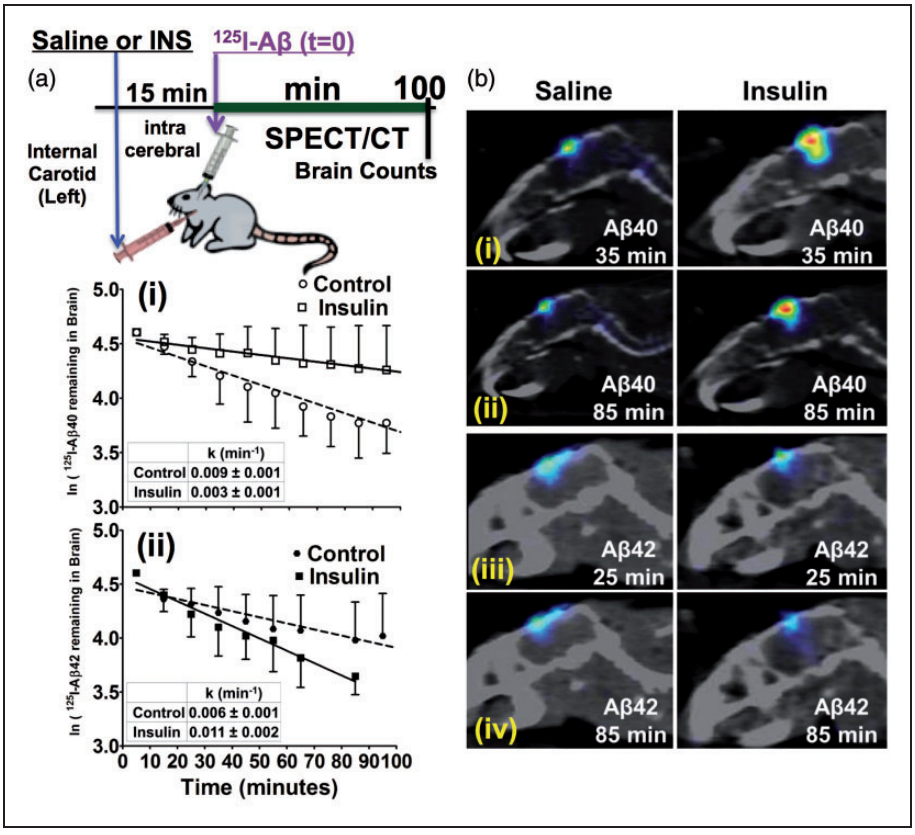

Figure 4. Brain-to-plasma clearance of ^{125}I-Aβ40 decreased, whereas ^{125}I-Aβ42 clearance increased with internal carotid administration of insulin in B6SJLF1 mice. (a) Normal saline or insulin (INS) was infused via the left internal carotid artery. Then, ^{125}I-Aβ was injected into the right hippocampus and imaged by SPECT/CT. Elimination of (i) ^{125}I-Aβ40 and (ii) ^{125}I-Aβ42 radioactivity from the injection site was fitted to a one-phase decay equation and the elimination rate constants (k) are presented in the inserted tables. Data are presented as mean ± S.D. (n = 4). F-test was conducted to check if the slopes of saline and insulin treated groups are significantly different. ^{125}I-Aβ40: $F(1,92) = 12.98$, $p < 0.001$ and ^{125}I-Aβ42 $F(1,65) = 6.73$, $p < 0.05$. (b) SPECT/CT images showing changes in (i) ^{125}I-Aβ40 at 35 min; (ii) ^{125}I-Aβ40 at 85 min; (iii) ^{125}I-Aβ42 radioactivity at 25 min; and (iv) ^{125}I-Aβ42 radioactivity at 85 min.

Moreover, insulin pre-treatment for either 20 min or 60 min increased the plasma membrane accumulation of RAGE compared to the untreated controls (Figure 6(b), panel-ii). Similarly, the P-gp accumulation increased with 20 and 60-min insulin exposure (Figure 6(b), panel-iii).

Insulin differentially modulates clathrin and caveolae-mediated endocytosis

Several reports have implicated insulin's role in intracellular trafficking.[21–23] Reports from our lab have shown that Aβ40 endocytosis is predominantly mediated by clathrin-mediated endocytosis, whereas the uptake of Aβ42 is primarily mediated by caveolae-mediated endocytosis.[24] Hence, we investigated the effect of insulin on the cellular endocytosis machinery in hCMEC/D3 cells, overexpressing the insulin receptor (IR-hCMEC/D3). Insulin pre-treatment increased the uptake of AF633-Trf (a classical marker for clathrin-mediated endocytosis) by 84% compared to the control cells as assessed by flow cytometry (Figure 7(a), panels-i and ii); and similar effects were evident in the confocal micrographs (Figure 7(a), panel-iii). However, insulin treatment decreased the uptake of AF647-CT (a marker for lipid rafts involved in caveolae-mediated endocytosis) by IR-hCMEC/D3 cell monolayers (Figure 7(b)).

Discussion

Recent clinical trials conducted in a small group of AD patients demonstrated the efficacy of intranasally administered insulin in improving memory and restoring normal amyloid levels in the brain.[25] Encouraged by these results, researchers have begun to investigate mechanisms of insulin action in plasma and brain, in the hope of discovering novel molecular targets for AD diagnosis and treatment. These investigations have shown that the peripheral insulin administration alters plasma Aβ clearance and increase Aβ levels in the brain interstitial fluid, whereas the intracerebral insulin administration does not have a detectable impact on

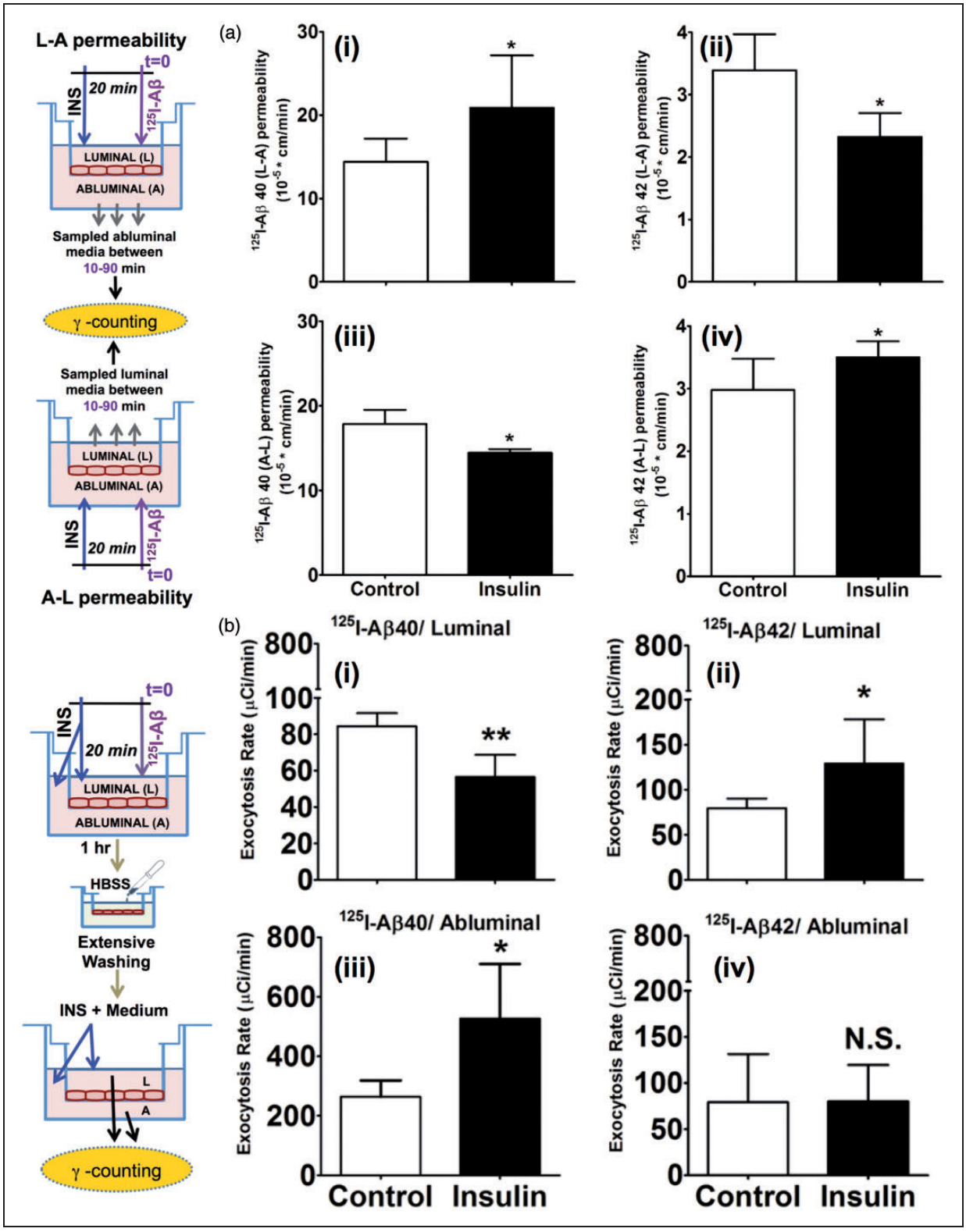

Figure 5. Insulin modulates ^{125}I-Aβ transcytosis and exocytosis in polarized hCMEC/D3 monolayers. (a) The L-A permeability of (i) ^{125}I-Aβ40 and (ii) ^{125}I-Aβ42 is presented as mean ± S.D. (n = 6). The A-L permeability of (iii) ^{125}I-Aβ40 and (iv) ^{125}I-Aβ42 is presented as mean ± S.D. (n = 6). *$p < 0.05$: Student's *t*-test. (b) Exocytosis of (i) ^{125}I-Aβ40 (control (n = 4), insulin (n = 4)) and (ii) ^{125}I-Aβ42 (control (n = 4), insulin (n = 4)) to the luminal (plasma) side. Exocytosis of (iii) ^{125}I-Aβ40 (control (n = 4), insulin (n = 3)) and (iv) ^{125}I-Aβ42 (control (n = 4), insulin (n = 4)) to the abluminal (brain) side. Data shown is mean ± S.D. *$p < 0.05$, **$p < 0.01$: Student's *t*-test.

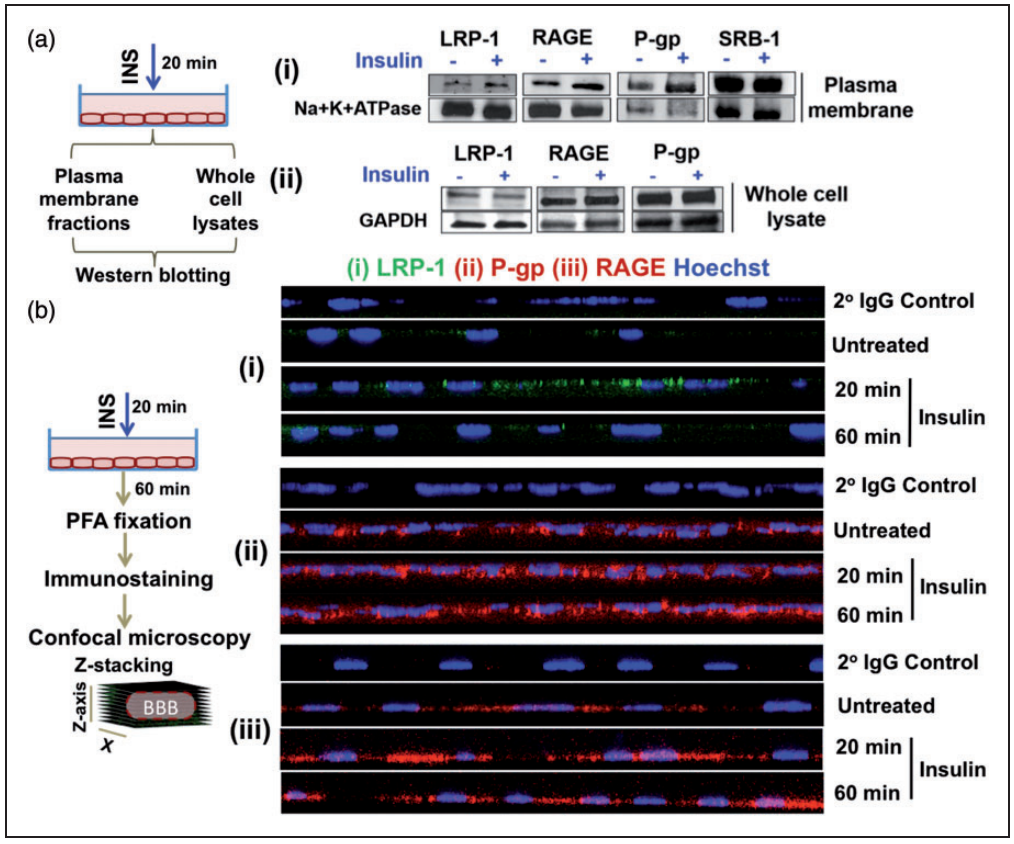

Figure 6. Insulin pre-treatment augments plasma membrane levels of putative Aβ receptors in polarized hCMEC/D3 cell monolayers. (a) *Western blotting*. Insulin increased the levels of LRP-1, P-gp and RAGE in the (i) plasma membrane fraction but not in the (ii) whole cell lysates. Loading controls: Na^+K^+ATPase (plasma membrane fraction) and GAPDH (whole cell lysates). (b) *Immunofluorescence*. Insulin exposure increased the expression of (i) LRP-1 (green); (ii) RAGE (red); and (iii) P-gp (red) in polarized hCMEC/D3 monolayers. Cells stained with secondary antibody alone (2° IgG Control) indicated background fluorescence. The cell nucleus is stained by Hoechst dye.

the brain Aβ levels.[10] The current study has verified and further resolved these findings by establishing the ability of peripheral insulin to differentially modulate Aβ40 and Aβ42 transcytosis at the BBB and affect their plasma and brain disposition.

Impact of peripheral insulin on plasma ^{125}I-Aβ kinetics

Exogenous insulin (1 IU) administration into systemic circulation increased the plasma clearance and decreased the plasma AUC (a parameter indicative of the extent of tissue exposure) of ^{125}I-Aβ40 (Figure 1(a) and (c)). This observation agrees with the previous findings that insulin facilitates the hepatic clearance of plasma Aβ40.[11] In contrast, the clearance of ^{125}I-Aβ42 decreased, and the plasma AUC increased with insulin administration (Figure 1(b) and (c)). The increase in plasma Aβ42 levels was shown to enhance hepatic insulin resistance.[26] Thus, changes in plasma insulin levels during the circadian cycles and chronic perturbations observed in metabolic disorders could decrease Aβ42 elimination from the plasma,[26] enhance its exposure to peripheral tissues, and beget peripheral insulin resistance which may exacerbate hyperinsulinemia.

Impact of insulin on brain ^{125}I-Aβ kinetics

With a 15-min infusion of 1 IU insulin, the plasma-to-brain influx of ^{125}I-Aβ40 increased, and that of ^{125}I-Aβ42 was reduced (Figure 2(a)). These trends were also verified by SPECT imaging. Gjedde–Patlak plots generated from the SPECT images provided estimates for the plasma-to-brain transfer rate constants (K_i) which are analogous to influx values obtained from the pharmacokinetic experiments. The K_i of ^{125}I-Aβ40 was found to be significantly greater than that of ^{125}I-Aβ42 (Figure 3). At higher doses (4.2 IU), the effect of insulin was clearly resolved in right and left hemispheres as well as in the brain regions which are affected in AD (cortex, hippocampus, caudate putamen, and thalamus[27,28]). Insulin administered via left

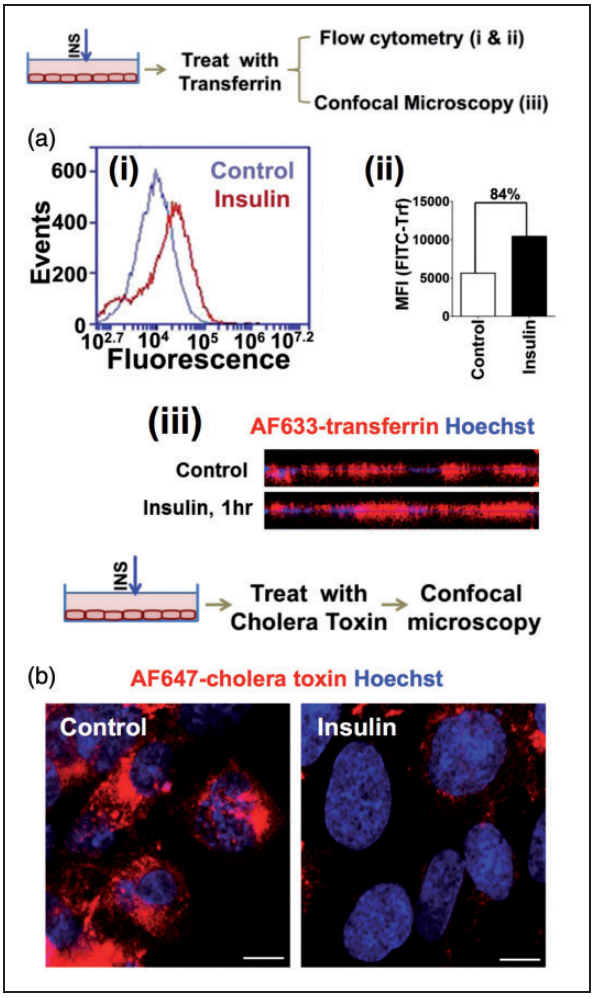

Figure 7. Insulin modulates endocytosis machinery in polarized hCMEC/D3 cell monolayers. (a) (i) Histogram of FITC-Transferrin (FITC-Trf) treated hCMEC/D3 cells overexpressing insulin receptor (IR-hCMEC/D3) as observed by flow cytometry. (ii) FITC-Trf fluorescence intensity (MFI) in IR-hCMEC/D3 monolayers with and without insulin exposure. (iii) Alexa Fluor® 633-transferrin uptake by confocal microscopy. The z-stack image along x-z axis was presented. The cell nucleus is stained by Hoechst dye. (b) Alexa Fluor® 647-cholera toxin uptake in insulin-treated IR-hCMEC/D3 cells observed by confocal microscopy. Scale bar – 10 μm.

internal carotid artery significantly increased the influx of ^{125}I-Aβ40 into these brain regions but reduced the influx of ^{125}I-Aβ42 (Figure 2(b)). Similar trends were apparent in the right hemisphere, but they are not statistically significant. Differences in the magnitude of insulin's effect on the right and left brain hemispheres could stem from differences in the insulin exposure. We estimated that the insulin infusion via the left internal carotid artery delivers twice as much insulin to the left hemisphere as to the right hemisphere within the experimental time-frame (Supplementary Figure 1). The observed effects of insulin on brain Aβ permeability are unlikely due to systemic pharmacological effects triggered by the insulin administration. If it were so, both hemispheres would have been equally affected.

Higher plasma insulin levels also differentially modulated the brain-to-plasma clearance of ^{125}I-Aβ40 and ^{125}I-Aβ42; the clearance of intracerebrally injected ^{125}I-Aβ40 was inhibited (Figure 4(a), panel (i) and (b), panels (i) and (ii)) but that of ^{125}I-Aβ42 was enhanced in insulin-exposed animals compared to the saline-treated controls (Figure 4(a), panel (ii) and (b), panels (iii) and (iv)). These results indicate that insulin spares Aβ40, but clears more toxic and amyloidogenic Aβ42 from the brain. Such changes in Aβ kinetics promoted by insulin could elevate Aβ40 levels and decrease relative Aβ42:40 ratios in the brain, which were shown to decrease amyloidogenesis[29] and impart neuroprotection.[30] These findings are also in agreement with the recent reports that peripheral insulin administration increased the accumulation of Aβ proteins in the brain interstitial fluid of $APP_{swe}/PS1\Delta E9$.[10] Although investigators of the study did not differentiate the accumulation of Aβ40 from Aβ42, it is easy to deduce that increase in the accumulation Aβ40, which is 10 times more abundant than Aβ42, could offset the decrease in Aβ42 accumulation, and show a net increase in brain Aβ accumulation.

Owing to beneficial effects reported by the direct nose-to-brain administration of insulin in AD patients,[25] it is important to separately consider the effects of luminal versus abluminal insulin exposure on Aβ trafficking. Shiiki et al.[9] have reported that intracerebral insulin administration in WT rats impaired ^{125}I-Aβ40 clearance from the brain. They also claimed that insulin does not affect putative Aβ40 trafficking receptors such as LRP-1, but altered the proteolytic degradation of Aβ40 by the insulin degrading enzyme (IDE).[9] It was purported that IDE primarily degrades monomeric Aβ40, whereas the degradation of amyloidogenic Aβ42 could follow multiple pathways.[31] The internal carotid insulin administration employed in this study may not facilitate enough insulin accumulation in the brain to adequately inhibit IDE and engender reduction in Aβ metabolism in the brain. Moreover, the differential impact of plasma insulin observed on the cerebral clearance of Aβ40 and Aβ42 suggests the substantial involvement of other clearance pathways. Recently, Stanley et al.[10] have reported that intracerebral insulin administration to $APP_{swe}/PS1\Delta E9$ did not change brain Aβ levels significantly. Differences in the observations made by these two groups could be due to the inability of intracerebrally injected insulin to rejuvenate already disrupted Aβ clearance pathways in $APP_{swe}/PS1\Delta E9$ model and/or due to the opposing effects of insulin on the brain clearances of Aβ40 and Aβ42. Stanley et al.[10] did not differentiate between

Aβ40 and Aβ42 when they assessed brain Aβ accumulation by microdialysis. Thus, increase in Aβ40 levels in the brain interstitial fluid (assessed) could be counteracted by the decrease in Aβ42 levels, and diminish the magnitude of overall effect.

Insulin modulates Aβ distribution between plasma and brain compartments, most likely by acting on the neurovascular unit, which constitutes neurons, glia (microglia and astrocytes), and vascular cells (BBB endothelium, pericytes, and vascular smooth muscle cells).[2] Insulin signaling is known to extend throughout these constituents of the neurovascular unit and is believed to regulate neurovascular function.[32,33] Although several pathways may be involved in clearing Aβ from the brain, the vascular clearance – mediated by the BBB endothelium, a highly specialized trafficking portal, and pericytes that modulate BBB signaling/trafficking – is the most predominant.[34] Insulin signaling pathways are shown to be critical for the functional coordination and communication between the endothelium and pericytes (reviewed by Richards et al.[8]). The deleterious consequences of hyperinsulinemia and insulin resistance – often observed in metabolic disorders – on the endothelium as well as pericytes[35,36] were shown to cause BBB dysfunction, which may impair brain Aβ clearance and also promote the influx of plasma Aβ into the brain (reviewed by Winkler et al.[37]).

Based on these observations made in vivo and the literature evidence, we hypothesized that insulin regulates Aβ trafficking at the BBB in L-A and A-L directions, and maintains Aβ40:Aβ42 ratios in plasma and brain compartments. Elucidating the mechanisms by which insulin conducts these functions in healthy subjects is critical to deciphering those pathological changes triggered by insulin resistance and hyperinsulinemia which are believed to aggravate AD pathology. Hence, the BBB trafficking of Aβ proteins in L-A and A-L directions and insulin's role in shepherding these processes was investigated in polarized hCMEC/D3 cell monolayers, which is a widely used human BBB model.[17] However, due to a lack of pericytes in this model, the impact of endothelial and pericytic interactions on Aβ trafficking and insulin's role in coordinating such interactions cannot be captured.

Insulin affects Aβ trafficking at the BBB endothelium

In agreement with our in vivo observations, the luminal uptake and L-A permeability of Aβ40 was enhanced, and that of Aβ42 was reduced in hCMEC/D3 monolayers exposed to luminal insulin (Figure 5(a)). In contrast, the A-L permeability of ^{125}I-Aβ40 was decreased, but the permeability of ^{125}I-Aβ42 was increased upon abluminal insulin exposure. However, the A-L permeability differences between control and insulin-treated monolayers are modest, which is likely due to the lack of pericytes in the model. Despite this limitation, the agreement between in vitro and in vivo findings confirm the earlier reports that the BBB plays a preeminent role in maintaining plasma and brain Aβ levels.[38] Moreover, our current findings suggest that insulin may modulate Aβ trafficking and regulate Aβ42:Aβ40 ratios in plasma and brain. Shifts in Aβ42:Aβ40 ratios observed in familial AD patients were claimed to be due to mutations in APP and/or PS1 genes.[39] However, the current manuscript suggests a possibility that aberrant Aβ42:Aβ40 ratios could arise due to perturbation in Aβ trafficking at the BBB. Thus, pathological conditions such as diabetes and obesity which are characterized by hyperinsulinemia, hyperlipidemia, and insulin resistance could engender pathological shifts in Aβ42:Aβ40 ratios.

We further investigated the effect of insulin on various stages of the transendothelial trafficking, primarily endocytosis and exocytosis, in hCMEC/D3 monolayers. The Aβ endocytosis on the luminal side of the BBB is mediated by the RAGE receptor, expressed on the luminal membrane.[40] RAGE is known to play a central role in insulin resistance and is implicated in vascular complications associated with diabetes.[41] The endocytosis of Aβ proteins on the abluminal side is handled by LRP-1, which is expressed on the abluminal membrane of the BBB.[42,43] LRP1 is also expressed on the pericyte membrane and aid in the endocytosis of Aβ proteins that are eventually degraded in the lysosomes. In addition, P-gp is expressed on the luminal membranes and is implicated in the brain Aβ clearance.[19] Upon luminal insulin exposure, the LRP-1, RAGE, and P-gp immunofluorescence transiently increased in the polarized hCMEC/D3 monolayers (Figure 6(b)). The western blots have shown that the luminal insulin exposure did not alter the cellular levels of these receptors/transporters in hCMEC/D3 endothelial monolayers, whereas the plasma membrane distribution of RAGE, LRP-1, and P-gp increased (Figure 6(a)). Similar studies were conducted on hepatocytes, where the luminal insulin exposure for various lengths of time was shown to induce the translocation of intracellular LRP-1 to the plasma membrane of hepatocytes and altered the peripheral clearance of Aβ40.[11] However, a manifestation of this phenomenon in the BBB endothelium has been addressed for the first time in the current study.

The Aβ endocytosis mediated by LRP1 and RAGE could progress via clathrin and/or caveolae-mediated pathways. Several studies have demonstrated the impact of insulin on these endocytotic processes in a variety of cells.[21,23] Further, insulin was shown to differentially modulate clathrin versus caveolae-mediated endocytosis of various ligands. For instance,

in adipocytes, insulin treatment decreased the endocytosis of cholera toxin B, which is internalized by caveolae-mediated endocytosis.[44] In contrast, the endocytosis of transferrin[44] and α-2 macroglobulin,[45] which is mediated by clathrin-mediated endocytosis, increased. In this study, we have shown that luminal insulin exposure enhanced the uptake of FITC-transferrin by BBB endothelial cells (Figure 7(a)), but reduced the uptake of AF647-cholera toxin B (Figure 7(b)), a caveolae-mediated endocytosis marker. This differential modulation of endocytotic processes by insulin could extend beyond the specific ligands and may affect the endocytosis of other proteins such as Aβ. We previously reported that Aβ40 uptake by endothelial cells is predominantly clathrin-mediated, whereas Aβ42 endocytosis is caveolae-mediated.[24,46] Hence, differential effects of insulin observed on the luminal uptake of Aβ40 and Aβ42 could be due to the ability of insulin to selectively enhance clathrin-mediated endocytosis and inhibit caveolae-mediated uptake.

However, effects of insulin on Aβ endocytosis do not entirely explain its differential impact on the brain clearances of Aβ40 and Aβ42. Insulin increases the expression of the endothelial LRP-1 receptor, which is purported to endocytose Aβ peptides on the abluminal side. Although Aβ40 has higher affinity to the LRP-1 receptor than does Aβ42,[47] it is not evident how insulin could decrease Aβ40 clearance from the brain. To resolve this dilemma, we also investigated the effect of insulin exposure on the exocytosis of Aβ internalized by the endothelial cells. Insulin preferentially promoted the exocytosis of the internalized ^{125}I-Aβ40 to the abluminal side, whereas the internalized ^{125}I-Aβ42 was exocytosed to the luminal side (Figure 5(b)). While this may, to some extent, reconcile differential effects of insulin on ^{125}I-Aβ40 and ^{125}I-Aβ42 transcytosis at the BBB, the mechanism of endothelial exocytosis modulated by insulin to manifest these trafficking changes remains to be investigated.

The current study points out the impact of plasma insulin on Aβ trafficking between plasma and brain compartments in healthy WT mice. Higher plasma insulin levels are observed in type-2 diabetes (T2DM) patients along with peripheral insulin resistance, and this could possibly affect the dynamic equilibrium between plasma and brain Aβ levels. However, T2DM is also associated with hyperglycemia, hyperlipidemia, hypertension, as well as cerebrovascular pathologies resulting from the destructive remodeling of endothelium, pericytes, and smooth muscle cells. Owing to the lack of understanding of how these comorbidities influence AD pathology, the current findings may not be sufficient to establish a causal link between AD and T2DM. Further studies employing relevant T2DM and AD models are warranted to fully realize the pathological consequences of T2DM sequelae on Aβ clearance and AD severity.

In summary, we have shown that intravenous insulin administration reduced the clearance and enhanced the plasma accumulation of Aβ42, which was previously shown to trigger peripheral insulin resistance. Moreover, systemic administration of exogenous insulin differentially modulated the bi-directional trafficking of Aβ40 and Aβ42 at the BBB and altered Aβ levels in the plasma and brain compartments. By invoking temporal and spatial changes in putative Aβ receptors and cellular transport machinery within the BBB endothelium, insulin promotes ^{125}I-Aβ40 accumulation in the brain but clears amyloidogenic ^{125}I-Aβ42. Hence, there may be an intricate signaling/trafficking apparatus at the BBB responsive to fluctuations in insulin levels, arising from the circadian cycles and nutritional status (e.g. fasting), and Aβ burden. Disruption of this regulatory network in cerebrovascular disease and metabolic disorders may exacerbate amyloidosis and insulin resistance, aggravate AD and CAA pathologies, and accelerate cognitive decline. Further studies are needed to verify these pathological consequences in WT and AD transgenic mouse models that manifest hyperinsulinemia and insulin resistance.

Funding

The author(s) disclosed receipt of the following financial support for the research, authorship, and/or publication of this article: Support of Minnesota Partnership for Biotechnology and Medical Genomics grant is acknowledged.

Declaration of conflicting interests

The author(s) declared no potential conflicts of interest with respect to the research, authorship, and/or publication of this article.

Authors' contributions

SKS, KMA, GLC, VS, RSO, TD performed the experiments, collected the data, participated in the data analysis. SKS, JFP, VJL, KKK made substantial contributions to conception and study design; data analysis and interpretation and, in drafting the manuscript. KKK managed the overall study. The final manuscript was reviewed, revised and approved by all the authors.

Supplementary material

Supplementary material for this paper can be found at the journal website: http://journals.sagepub.com/home/jcb

References

1. Jack CR Jr, Knopman DS, Jagust WJ, et al. Tracking pathophysiological processes in Alzheimer's disease: an

updated hypothetical model of dynamic biomarkers. *Lancet Neurol* 2013; 12: 207–216.
2. Sagare AP, Bell RD and Zlokovic BV. Neurovascular dysfunction and faulty amyloid beta-peptide clearance in Alzheimer disease. *Cold Spring Harbor Perspect Med* 2012; 2: a011452.
3. De Felice FG. Alzheimer's disease and insulin resistance: translating basic science into clinical applications. *J Clin Invest* 2013; 123: 531–539.
4. de and la Torre JC. Alzheimer disease as a vascular disorder: nosological evidence. *Stroke* 2002; 33: 1152–1162.
5. Fernandez-Klett F, Offenhauser N, Dirnagl U, et al. Pericytes in capillaries are contractile in vivo, but arterioles mediate functional hyperemia in the mouse brain. *Proc Natl Acad Sci U S A* 2010; 107: 22290–22295.
6. Armulik A, Genove G, Mae M, et al. Pericytes regulate the blood-brain barrier. *Nature* 2010; 468: 557–561.
7. Bell RD, Winkler EA, Sagare AP, et al. Pericytes control key neurovascular functions and neuronal phenotype in the adult brain and during brain aging. *Neuron* 2010; 68: 409–427.
8. Richards OC, Raines SM and Attie AD. The role of blood vessels, endothelial cells, and vascular pericytes in insulin secretion and peripheral insulin action. *Endocrine Rev* 2010; 31: 343–363.
9. Shiiki T, Ohtsuki S, Kurihara A, et al. Brain insulin impairs amyloid-beta(1-40) clearance from the brain. *J Neurosci* 2004; 24: 9632–9637.
10. Stanley M, Macauley SL, Caesar EE, et al. The Effects of peripheral and central high insulin on brain insulin signaling and amyloid-beta in young and Old APP/PS1 mice. *J Neurosci* 2016; 36: 11704–11715.
11. Tamaki C, Ohtsuki S and Terasaki T. Insulin facilitates the hepatic clearance of plasma amyloid beta-peptide (1 40) by intracellular translocation of low-density lipoprotein receptor-related protein 1 (LRP-1) to the plasma membrane in hepatocytes. *Mol Pharmacol* 2007; 72: 850–855.
12. Poduslo JF, Curran GL, Wengenack TM, et al. Permeability of proteins at the blood-brain barrier in the normal adult mouse and double transgenic mouse model of Alzheimer's disease. *Neurobiol Dis* 2001; 8: 555–567.
13. Jaruszewski KM, Curran GL, Swaminathan SK, et al. Multimodal nanoprobes to target cerebrovascular amyloid in Alzheimer's disease brain. *Biomaterials* 2014; 35: 1967–1976.
14. Patlak CS and Blasberg RG. Graphical evaluation of blood-to-brain transfer constants from multiple-time uptake data. *J Cereb Blood Flow Metab* 1985; 5: 584–590.
15. Patlak CS, Blasberg RG and Fenstermacher JD. Graphical evaluation of blood-to-brain transfer constants from multiple-time uptake data. *J Cereb Blood Flow Metab* 1983; 3: 1–7.
16. Gjedde A. Calculation of cerebral glucose phosphorylation from brain uptake of glucose analogs in vivo: a re-examination. *Brain Res* 1982; 257: 237–274.
17. Weksler B, Romero IA and Couraud PO. The hCMEC/D3 cell line as a model of the human blood brain barrier. *Fluids Barriers CNS* 2013; 10: 16.
18. Deane R, Bell RD, Sagare A, et al. Clearance of amyloid-beta peptide across the blood-brain barrier: implication for therapies in Alzheimer's disease. *CNS Neurol Disord Drug Targets* 2009; 8: 16–30.
19. Hartz AM, Miller DS and Bauer B. Restoring blood-brain barrier P-glycoprotein reduces brain amyloid-beta in a mouse model of Alzheimer's disease. *Mol Pharmacol* 2010; 77: 715–723.
20. Thanopoulou K, Fragkouli A, Stylianopoulou F, et al. Scavenger receptor class B type I (SR-BI) regulates perivascular macrophages and modifies amyloid pathology in an Alzheimer mouse model. *Proc Natl Acad Sci U S A* 2010; 107: 20816–20821.
21. Solano DC, Sironi M, Bonfini C, et al. Insulin regulates soluble amyloid precursor protein release via phosphatidyl inositol 3 kinase-dependent pathway. *FASEB J* 2000; 14: 1015–1022.
22. Watson RT, Kanzaki M and Pessin JE. Regulated membrane trafficking of the insulin-responsive glucose transporter 4 in adipocytes. *Endocrine Rev* 2004; 25: 177–204.
23. Gasparini L, Gouras GK, Wang R, et al. Stimulation of beta-amyloid precursor protein trafficking by insulin reduces intraneuronal beta-amyloid and requires mitogen-activated protein kinase signaling. *J Neurosci* 2001; 21: 2561–2570.
24. Sharda N, Omtri R, Jaruszweki K et al. Trafficking kinetics of amyloid beta protein at the blood brain barrier in alzheimer's disease. AAPS 2015, Orlando. Available at: http://abstracts.aaps.org/SecureView/AAPSJournal/radrunf2z04.pdf.
25. Craft S, Baker LD, Montine TJ, et al. Intranasal insulin therapy for Alzheimer disease and amnestic mild cognitive impairment: a pilot clinical trial. *Arch Neurol* 2012; 69: 29–38.
26. Zhang Y, Zhou B, Deng B, et al. Amyloid-beta induces hepatic insulin resistance in vivo via JAK2. *Diabetes* 2013; 62: 1159–1166.
27. Aggleton JP, Pralus A, Nelson AJ, et al. Thalamic pathology and memory loss in early Alzheimer's disease: moving the focus from the medial temporal lobe to Papez circuit. *Brain* 2016; 139(Pt 7): 1877–1890.
28. de Jong LW, van der Hiele K, Veer IM, et al. Strongly reduced volumes of putamen and thalamus in Alzheimer's disease: an MRI study. *Brain* 2008; 131(Pt 12): 3277–3285.
29. Kim J, Onstead L, Randle S, et al. Abeta40 inhibits amyloid deposition in vivo. *J Neurosci* 2007; 27: 627–633.
30. Chen Y and Dong C. Abeta40 promotes neuronal cell fate in neural progenitor cells. *Cell Death Diff* 2009; 16: 386–394.
31. Farris W, Mansourian S, Chang Y, et al. Insulin-degrading enzyme regulates the levels of insulin, amyloid beta-protein, and the beta-amyloid precursor protein intracellular domain in vivo. *Proc Natl Acad Sci U S A* 2003; 100: 4162–4167.
32. Liu CC, Hu J, Tsai CW, et al. Neuronal LRP1 regulates glucose metabolism and insulin signaling in the brain. *J Neurosci* 2015; 35: 5851–5859.
33. Garcia-Caceres C, Quarta C, Varela L, et al. Astrocytic insulin signaling couples brain glucose uptake with nutrient availability. *Cell* 2016; 166: 867–880.

34. Shibata M, Yamada S, Kumar SR, et al. Clearance of Alzheimer's amyloid-ss(1-40) peptide from brain by LDL receptor-related protein-1 at the blood-brain barrier. *J Clin Invest* 2000; 106: 1489–1499.
35. Siemionow M and Demir Y. Diabetic neuropathy: pathogenesis and treatment. *J Reconst Microsurg* 2004; 20: 241–252.
36. Tilton RG, Hoffmann PL, Kilo C, et al. Pericyte degeneration and basement membrane thickening in skeletal muscle capillaries of human diabetics. *Diabetes* 1981; 30: 326–334.
37. Winkler EA, Sagare AP and Zlokovic BV. The pericyte: a forgotten cell type with important implications for Alzheimer's disease? *Brain Pathol* 2014; 24: 371–386.
38. Deane R, Sagare A and Zlokovic BV. The role of the cell surface LRP and soluble LRP in blood-brain barrier Abeta clearance in Alzheimer's disease. *Curr Pharmaceut Des* 2008; 14: 1601–1605.
39. Hellstrom-Lindahl E, Viitanen M and Marutle A. Comparison of Abeta levels in the brain of familial and sporadic Alzheimer's disease. *Neurochem Int* 2009; 55: 243–252.
40. Mackic JB, Stins M, McComb JG, et al. Human blood-brain barrier receptors for Alzheimer's amyloid-beta 1- 40. Asymmetrical binding, endocytosis, and transcytosis at the apical side of brain microvascular endothelial cell monolayer. *J Clin Invest* 1998; 102: 734–743.
41. Ramasamy R, Yan SF and Schmidt AM. Receptor for AGE (RAGE): signaling mechanisms in the pathogenesis of diabetes and its complications. *Ann N Y Acad Sci* 2011; 1243: 88–102.
42. Silverberg GD, Messier AA, Miller MC, et al. Amyloid efflux transporter expression at the blood-brain barrier declines in normal aging. *J Neuropathol Exp Neurol* 2010; 69: 1034–1043.
43. Storck SE, Meister S, Nahrath J, et al. Endothelial LRP1 transports amyloid-beta(1-42) across the blood-brain barrier. *J Clin Invest* 2016; 126: 123–136.
44. Blot V and McGraw TE. GLUT4 is internalized by a cholesterol-dependent nystatin-sensitive mechanism inhibited by insulin. *EMBO J* 2006; 25: 5648–5658.
45. Habtemichael EN, Brewer PD, Romenskaia I, et al. Kinetic evidence that Glut4 follows different endocytic pathways than the receptors for transferrin and alpha2-macroglobulin. *J Biol Chem* 2011; 286: 10115–10125.
46. Omtri RS, Davidson MW, Arumugam B, et al. Differences in the cellular uptake and intracellular itineraries of amyloid beta proteins 40 and 42: ramifications for the Alzheimer's drug discovery. *Mol Pharm* 2012; 9: 1887–1897.
47. Deane R, Wu Z, Sagare A, et al. LRP/amyloid beta-peptide interaction mediates differential brain efflux of Abeta isoforms. *Neuron* 2004; 43: 333–344.